

Topological superconductivity in quasicrystals

Rasoul Ghadimi,¹ Takanori Sugimoto,^{1,2} K. Tanaka,³ and Takami Tohyama¹

¹*Department of Applied Physics, Tokyo University of Science, Tokyo 125-8585, Japan*

²*Advanced Science Research Center, Japan Atomic Energy Agency, Tokai, Ibaraki 319-1195, Japan*

³*Department of Physics and Engineering Physics,*

and Centre for Quantum Topology and Its Applications (quanTA),

University of Saskatchewan, 116 Science Place, Saskatoon, Saskatchewan, Canada S7N 5E2

(Dated: December 22, 2024)

We propose realization of non-Abelian topological superconductivity in two-dimensional quasicrystals by the same mechanism as in crystalline counterparts. Specifically, we study a two-dimensional electron gas in Penrose and Ammann-Beenker quasicrystals with Rashba spin-orbit coupling, perpendicular Zeeman magnetic field, and conventional s -wave superconductivity. We find that topological superconductivity with broken time-reversal symmetry is realized in both Penrose and Ammann-Beenker quasicrystals at low filling, where the Bott index is unity. The topological nature of this phase is confirmed by the existence of a zero-energy surface bound state and the chiral propagation of a wave packet projected onto the midgap bound state along the surfaces. Furthermore, we confirm the existence of a single Majorana zero mode each in a vortex at the center of the system and along the surfaces, signifying the non-Abelian character of the system when the Bott index is unity.

Introduction—Since the first discovery of three-dimensional topological insulators about a decade ago [1, 2], a wide variety of topological materials has been discovered theoretically as well as experimentally [3–6]. Classification of topological materials [7] is not only limited to crystalline systems, but also has been extended to include disordered [8], amorphous [9] and quasicrystal materials. Quasicrystals [10, 11], which present phases of matter with long-range structural order without periodicity [12], have brought about new research into topology in condensed matter systems [13, 14]. Topological properties of quasicrystals [15, 16] have been investigated in connection with the quantum Hall effect [17–19], the quantum spin Hall effect [20, 21], higher-order topological phases [22, 23], and superconductivity [24–28]. Moreover, recent technical advances for experimental realization of two-dimensional (2D) quasicrystals, either in optical lattices [29, 30] or by means of crystal growth technologies [31–36], have enabled studies of novel quantum phenomena in actual quasicrystals.

One of the most significant properties of topological materials is the existence of Majorana fermions in topological superconductors [4]. The capability of creating and manipulating Majorana fermions in a solid device may well open the door to realizing stable and scalable quantum computation that is topologically protected [6]. In a one-dimensional system presenting topological superconductivity (TSC) as in the Kitaev model [37], zero-energy Majorana fermions appear at the two ends of the system [38, 39]. In a 2D topological superconductor, a Majorana zero mode can appear not only along a surface [40], but also in the vortex core [41]. 2D TSC with broken time-reversal symmetry has been proposed to be realized in an ultracold Fermi gas [42, 43] and heterostructure made of conventional materials [4, 44, 45], and has been achieved in a Pb/Co island on Si(111) [40]. Neces-

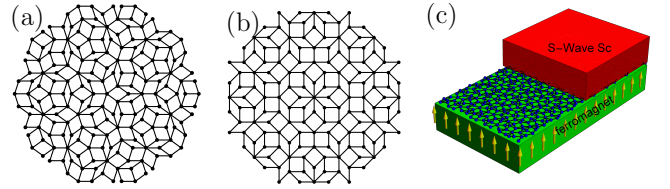


FIG. 1. (a) Penrose and (b) Ammann-Beenker quasicrystals studied in this work. (c) A schematic setup for realizing a topological quasicrystal superconductor in heterostructure.

sary ingredients are 2D s -wave superconductivity [46–49], Rashba spin-orbit coupling (RSOC) [50–52], and perpendicular Zeeman magnetic field (PZMF). RSOC can be enhanced or induced by proximity effects in heterostructure [53–57].

In our previous work [58], we have studied the topological phase diagram of the Fibonacci-Kitaev model as an example of simplest one-dimensional quasicrystalline topological superconductors. We have found that quasicrystal structure has a profound effect on the topological phase diagram, making it fractal. One might now ask, what will happen if the spatial dimension increases from one to two? Can TSC be stable even in 2D quasicrystals? In order to answer these questions, in this Letter we apply the method of realizing 2D TSC with broken time-reversal symmetry [42, 43] to quasicrystals. Specifically, we study Penrose and Ammann-Beenker quasicrystals (see Figs. 1(a) and (b)) at low filling with RSOC, PZMF and s -wave superconducting pairing. We find that irrespective of the aperiodicity of a quasicrystal, TSC is realized as in a square lattice with translational invariance. This finding is obtained by calculating the Bott index as a topological invariant in the system [8, 20, 21] and confirming the existence of a Majorana zero mode in a vortex and along the surfaces in the topological phase

where the Bott index is unity.

Model—In this Letter, we focus on 2D Penrose and Ammann-Beenker quasicrystals as illustrated in Figs. 1(a) and (b). Our results can be generalized readily for other types of 2D quasicrystals. We generalize the tight-binding model [42, 43] for a quasicrystal:

$$\mathcal{H} = \frac{1}{2} \sum_{ij} (c_i^\dagger \ c_i) H \begin{pmatrix} c_j \\ c_j^\dagger \end{pmatrix}, \quad H = \begin{pmatrix} \mathbf{h} & \Delta \\ \Delta^\dagger & -\mathbf{h}^* \end{pmatrix}, \quad (1)$$

where $c_i = (c_{1\uparrow} \ c_{1\downarrow} \dots)$ is the spinor annihilation operator for electrons and the normal-state Hamiltonian is

$$[\mathbf{h}]_{i\alpha,j\beta} = \left[(t_{ij} - \mu\delta_{ij})\sigma_0 + h_z\delta_{ij}\sigma_3 + V_{ij}\vec{e}_z \cdot \vec{\sigma} \times \vec{R}_{ij}\sigma_2 \right]_{\alpha\beta} \quad (2)$$

with the Pauli matrices $\vec{\sigma} = (\sigma_1, \sigma_2, \sigma_3)$ acting in spin space and $\sigma_0 = \mathbf{1}_2$ the 2×2 identity matrix. We consider the vertex model [59], where the sites $\{i\}$ are defined on vertices in the quasicrystal and $\vec{R}_{ij} = \vec{R}_i - \vec{R}_j$ connects sites i and j . We consider nearest-neighbor hopping only, $t_{ij} = t_{\langle ij \rangle} \equiv -t$, and $V_{ij} = V_{\langle ij \rangle} \equiv V$ is the coupling constant of RSOC, where $\langle \rangle$ indicates nearest-neighbor links. PZMF and the chemical potential are denoted as h_z and μ , respectively. The off-diagonal elements are given by

$$[\Delta]_{i\alpha,j\beta} = [\delta_{ij}\Delta\iota\sigma_2]_{\alpha\beta}, \quad (3)$$

where $\iota = \sqrt{-1}$ and Δ is the s -wave superconducting order parameter. A possible setup of the system is illustrated in Fig. 1(c), where PZMF and s -wave superconductivity are induced by proximity to a ferromagnetic insulator and a conventional superconductor, respectively. RSOC can be enhanced or induced by the ferromagnetic insulator [60] or the superconductor [61, 62]. To explore the properties of such a system, we numerically diagonalize the BdG Hamiltonian in Eq. (1) to find quasiparticle energy spectrum and wavefunctions [63]:

$$H|\psi_\lambda\rangle = \epsilon_\lambda|\psi_\lambda\rangle. \quad (4)$$

The topological phases in a square lattice with translational symmetry have been classified in Ref. [43] according to the first Chern number [64], $\nu \in \mathbb{Z}$ [7], where the system is in trivial, Abelian, and non-Abelian phase when $\nu = 0$, $\nu = -2$, and $\nu = \pm 1$, respectively. For the chemical potential $\mu \leq -2t$ and for large enough PZMF, the system can have a single noninteracting Fermi surface, and non-Abelian phase with $\nu = 1$ is realized when $\Delta^2 < h_z^2 - (W + \mu)^2$, where Δ is taken to be real and $W = 4t$ is half of the bandwidth in the absence of RSOC and PZMF in the normal state. This phase hosts a zero-energy Majorana fermion as a single edge mode per surface or bound state in a vortex [43, 65, 66].

In the following, we set

$$V = 0.5t, \quad h_z = 0.5t, \quad \Delta = 0.2t,$$

and probe topological phase transitions by varying the chemical potential in the low-filling limit.

Energy gap, Bott index, and edge modes—The Bott index [8, 67] is one of the topological invariants that are equivalent to the first Chern number, previously used [20, 21, 24, 68] to explore nontrivial states of a quasicrystal. In order to calculate the Bott index, we first obtain the quasiparticle wavefunctions. Exploiting the particle-hole symmetry of Eq. (4), we define the occupation projector onto the wavefunctions corresponding to negative energy,

$$P = \sum_{\epsilon_\lambda < 0} |\psi_\lambda\rangle \langle \psi_\lambda|. \quad (5)$$

In terms of this projector and $Q = I - P$, with I the identity operator, we can define the projected position operators,

$$U_X = P e^{i2\pi X} P + Q, \quad U_Y = P e^{i2\pi Y} P + Q, \quad (6)$$

where

$$X = \text{Diag}[x_1, x_1, \dots, x_N, x_N, \dots, x_1, x_1, \dots, x_N, x_N]. \quad (7)$$

Here N is the total number of vertices, x_i is the x coordinate of the i th vertex rescaled to $[0, 1]$, and similarly for Y . The Bott index is defined by

$$B = \frac{1}{2\pi} \text{Im}(\text{Tr}[\log(U_Y U_X U_Y^\dagger U_X^\dagger)]), \quad (8)$$

which is quantized to be a nonzero integer (zero) in topologically nontrivial (trivial) phase. We use the periodic boundary condition (PBC) for calculation of the Bott index. In nontrivial topological states the periodic and open boundary conditions (OBC) result in a gapful and gapless energy spectrum, respectively. The latter is a direct consequence of the bulk-boundary correspondence [69]. Application of PBC to Ammann-Beenker quasicrystal supercells is relatively simple. We first identify a large square-lattice portion of the quasicrystal that has similar edges, and then apply PBC to each pair of two parallel edges. For Penrose quasicrystals we use the approximant method [70].

In Fig. 2(a-c) we present the Bott index and the lowest quasiparticle excitation energy as a function of the chemical potential μ for a 54×54 square lattice, Penrose (3571 vertices) and Ammann-Beenker (2869 vertices) quasicrystals. It can be seen that irrespective of the crystal structure, the energy gap closes twice as μ is increased in the region shown, where the Bott index B changes first from zero to unity and then back to zero. $B = 1$ for $-W - \sqrt{h_z^2 - \Delta^2} < \mu < -W + \sqrt{h_z^2 - \Delta^2}$, where W is half of the normal-state bandwidth in the absence of RSOC and PZMF, *regardless* of the crystal structure. These two critical values of μ are indicated by two vertical lines for each system in Fig. 2(a-c). We have

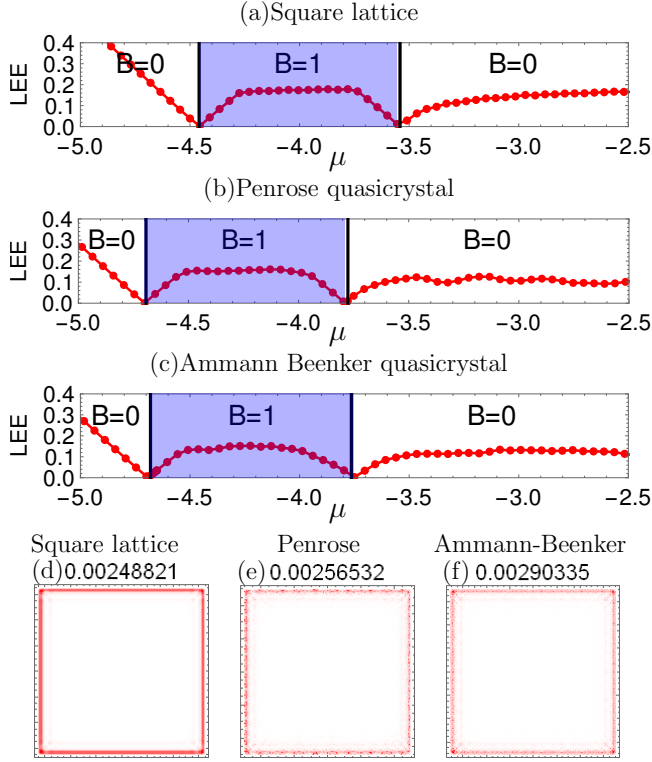


FIG. 2. Lowest excitation energy (LEE) is plotted as a function of the chemical potential for (a) a square lattice (2916 vertices), (b) Penrose (3571 vertices) and (c) Ammann-Beenker (2869 vertices) quasicrystals with PBC. The probability distribution of the lowest-energy excitation in a (d) square lattice (17161 vertices), (e) Penrose (18643 vertices) and (f) Ammann-Beenker (16437 vertices) quasicrystals with OBC for $\mu = -4.25t$. The darker (red) color implies higher probability. The energy of each state is shown above each plot.

confirmed these phase transitions for different combinations of parameter values (V , h_z , Δ) and system size.

The bulk-boundary correspondence implies the existence of a gapless bound state per surface in the topological phase with $B = 1$. This is illustrated in Fig. 2(d-f), where the probability distribution is plotted for the lowest-energy state in a 131×131 square lattice, Penrose (18643 vertices) and Ammann-Beenker (16437 vertices) quasicrystals for $\mu = -4.25t$. The energy ($\sim 10^{-3}t$) for each state is shown above each plot. Clearly these states are strongly localized along the surfaces, and the energy of these states approaches zero as the system size increases. In the thermodynamic limit, these midgap surface bound states have a continuous excitation spectrum. In contrast, in trivial phase there is no such surface bound state and the wavefunction distribution depends drastically on μ and shape of the system.

Chiral propagation—Because of the chiral nature of edge modes in a square lattice [43, 65], we anticipate the unidirectional propagation of the midgap surface bound states. To see this, we project an initial state $|\psi_0\rangle$ localized

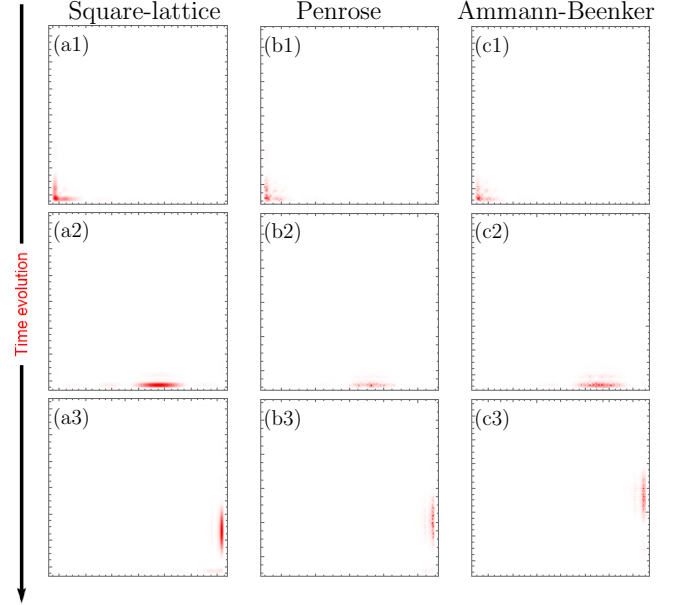


FIG. 3. Time evolution of the chiral propagation of a surface bound state is illustrated for the same systems as in Fig. 2(d-f); for (a1-a3) a square lattice, (b1-b3) Penrose and (c1-c3) Ammann-Beenker quasicrystals for $\mu = -4.25t$.

around an edge site onto the lowest-energy midgap state. We then allow the system to evolve with time by applying the time evolution operator $\exp(-iTH)$ at time T . If the system supports chiral edge modes, the initial state would propagate along the boundary [18, 30, 71]. In Fig. 3 the time-lapse propagation of the initial state is presented for the first few time steps, $\Delta T = 50t$. We can see that despite the aperiodicity, the wave packet propagates along the surface boundary in both quasicrystals as in a square lattice. On the contrary, in trivial phase an initial wave packet quickly disperses into the bulk of the system.

Vortex bound states—It is possible to directly confirm the existence of Majorana zero modes by introducing a vortex in the system. For this purpose, we include a vortex as a local phase winding in the order parameter in the middle of the crystal. We set the pairing amplitude to zero at the vortex center to avoid ambiguity in the pairing phase, while assuming no radial dependence in the amplitude or phase. Introducing a vortex induces the Caroli-de Gennes-Matricon (CdGM) bound states localized in the vortex core. The energy of the CdGM states are quantized [72, 73] in terms of the so-called minigap, $\sim \Delta E_0/k_F^2$, where E_0 is the bulk spectral gap and k_F is the magnitude of the Fermi wave vector [63, 66]. While it is unclear as to how well this common formula applies to the CdGM levels in the current system with RSOC and PZMF, we expect the minigap to be dependent on μ for a given V , h_z , and Δ . In the $B = 1$ phase, we additionally find a zero-energy Majorana bound state in

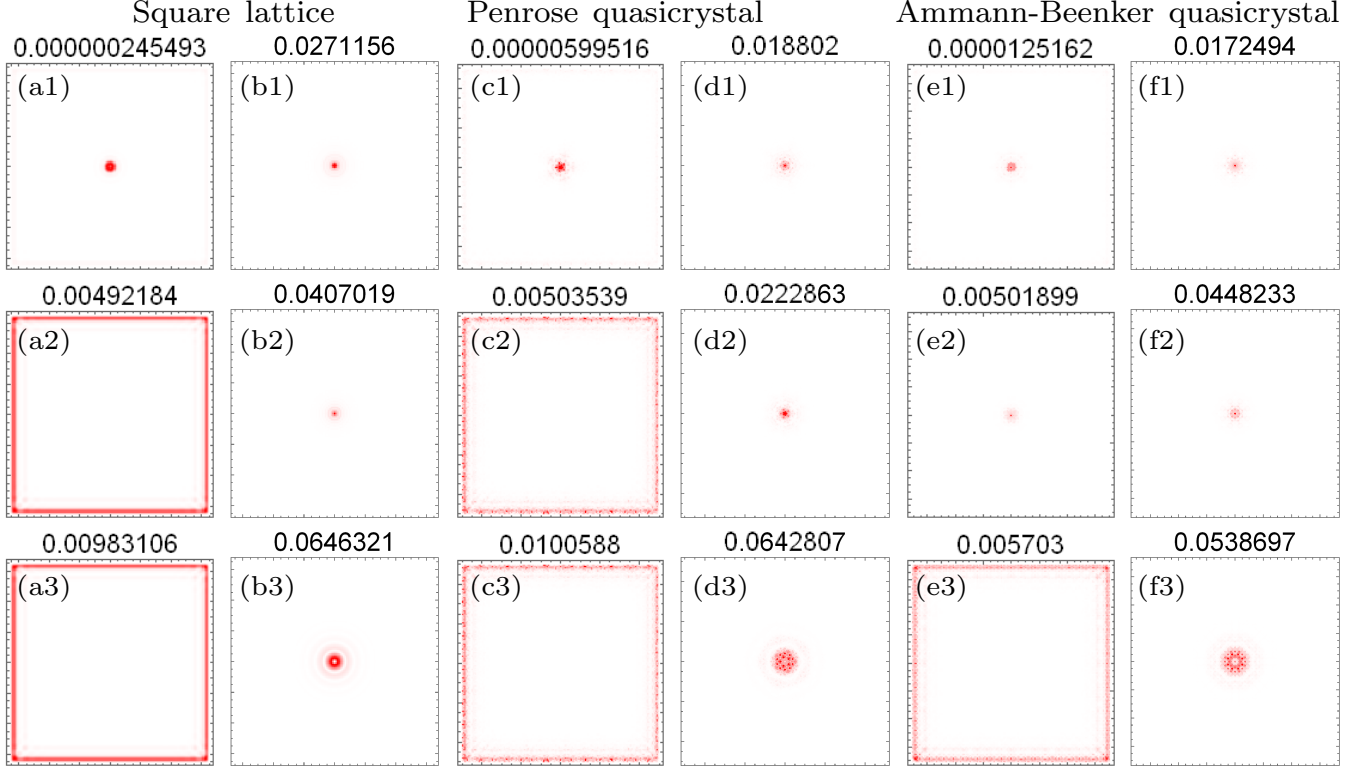


FIG. 4. The probability distribution of the four lowest-energy excitations is plotted for a square lattice in the (a1-a3) topologically nontrivial ($\mu = -4.25t$) and (b1-b3) trivial ($\mu = -3t$) phase, Penrose quasicrystal in the (c1-c3) topologically nontrivial ($\mu = -4.25t$) and (d1-d3) trivial ($\mu = -3.5t$) phase, and Ammann-Beenker quasicrystal in the (e1-e3) topologically nontrivial ($\mu = -4.25t$) and (f1-f3) trivial ($\mu = -3.5t$) phase. The number of vertices in each system is the same as for the respective system presented in Fig. 2(d-f). The excitation energy of each state is shown above each plot.

the vortex core, which is clearly distinct from the CdGM states, as its energy is approximately zero regardless of μ and approaches zero as the system size increases. In contrast, the lowest energy of the vortex bound states in trivial phase strongly depends on μ .

With a vortex at the center of the system with OBC, the BdG equations (4) yield two zero-energy solutions, numerically with energy $\pm\epsilon$ where $\epsilon \ll t$. In Fig. 4 we plot the probability distribution of the three lowest-positive-energy states for two values of μ each for a square lattice (17161 vertices), Penrose (18643 vertices) and Ammann-Beenker (16437 vertices) quasicrystals, such that $B = 1$ for one value of μ ($\mu = -4.25t$ for all systems) and $B = 0$ for the other ($\mu = -3t$ for the square lattice and $\mu = -3.5t$ for the quasicrystals). The energy of each state is shown above each plot. Although it may not be discernible due to the relatively large system size, the zero-energy state in all three systems shown in Fig. 4(a1,c1,e1) has half of its probability distributed along the surfaces and the other half concentrated around the vortex center. This is also the case for the other zero-energy state (numerically with slightly negative energy) in each system. Furthermore, each of the zero-energy state has equal probabilities being an electron and a

hole. Thus, analogously to the non-Abelian phase in the square lattice, a Majorana zero mode exists per vortex or surface in both kinds of quasicrystals in the topological phase with $B = 1$. It is interesting to note that second-lowest-energy excitation in the $B = 1$ phase is a surface state in the square lattice and Penrose quasicrystal, while it is a CdGM state in the Ammann-Beenker quasicrystal. The quasicrystal structure is reflected in the CdGM wavefunctions, which have five- and eight-fold symmetry in the Penrose (Fig. 4(d1-d3)) and Ammann-Beenker (Fig. 4(f1-f3)) systems, respectively, in accordance with the five- and eight-fold symmetry of the quasicrystal.

Conclusion—In this work, we have extended the 2D TSC model with broken time-reversal symmetry to 2D quasicrystals. We have shown that despite the aperiodicity, nontrivial topological phase can be realized in Penrose and Ammann-Beenker quasicrystals at low filling, where the Bott index is nonzero. When the Bott index $B = 1$, both Penrose and Ammann-Beenker quasicrystals host a chiral surface bound state. Furthermore, by introducing a vortex at the center of the system in the $B = 1$ phase, we have found two zero-energy, highly localized bound states, one along the surfaces and the other around the vortex center, irrespective of the underlying crystal

structure. In contrast to the CdGM vortex bound states in trivial phase, the lowest energy of the vortex bound states in topological phase remains approximately zero regardless of the value of the chemical potential. We have further confirmed (not shown) that each of these bound states is a Majorana zero mode with half of its probability being a particle and the other half a hole. Our results indicate that a new setup of heterostructure using quasicrystals as in Fig. 1(c) is possible for realizing two-dimensional TSC.

This work was supported by the Japan Society for the Promotion of Science, KAKENHI (Grant No. JP19H05821), and partially by the Natural Sciences and Engineering Research Council of Canada. K.T. is grateful to the Tokyo University of Science for hospitality, where part of the research was performed.

-
- [1] M. Z. Hasan and C. L. Kane, *Rev. Mod. Phys.* **82**, 3045 (2010).
 - [2] M. Z. Hasan and J. E. Moore, *Ann. Rev. Cond. Matt. Phys.* **2**, 55 (2011).
 - [3] X.-L. Qi and S.-C. Zhang, *Rev. Mod. Phys.* **83**, 1057 (2011).
 - [4] J. Alicea, *Rep. Prog. Phys.* **75**, 076501 (2012).
 - [5] Y. Ando and L. Fu, *Ann. Rev. Cond. Matt. Phys.* **6**, 361 (2015).
 - [6] M. Sato and Y. Ando, *Rep. Prog. Phys.* **80**, 076501 (2017).
 - [7] A. P. Schnyder, S. Ryu, A. Furusaki, and A. W. W. Ludwig, *Phys. Rev. B* **78**, 195125 (2008).
 - [8] T. A. Loring and M. B. Hastings, *Europhys. Lett.* **92**, 67004 (2010).
 - [9] N. P. Mitchell, L. M. Nash, D. Hexner, A. M. Turner, and W. T. M. Irvine, *Nat. Phys.* **14**, 380 (2018).
 - [10] D. Levine and P. J. Steinhardt, *Phys. Rev. B* **34**, 596 (1986).
 - [11] J. E. S. Socolar and P. J. Steinhardt, *Phys. Rev. B* **34**, 617 (1986).
 - [12] D. Shechtman, I. Blech, D. Gratias, and J. W. Cahn, *Phys. Rev. Lett.* **53**, 1951 (1984).
 - [13] Y. E. Kraus, Y. Lahini, Z. Ringel, M. Verbin, and O. Zilberberg, *Phys. Rev. Lett.* **109**, 106402 (2012).
 - [14] K. A. Madsen, E. J. Bergholtz, and P. W. Brouwer, *Phys. Rev. B* **88**, 125118 (2013).
 - [15] M. Verbin, O. Zilberberg, Y. E. Kraus, Y. Lahini, and Y. Silberberg, *Phys. Rev. Lett.* **110**, 076403 (2013).
 - [16] A. Dureau, E. Levy, M. B. Aguilera, R. Bouganne, E. Akkermans, F. Gerbier, and J. Beugnon, *Phys. Rev. Lett.* **119**, 215304 (2017).
 - [17] Y. E. Kraus, Z. Ringel, and O. Zilberberg, *Phys. Rev. Lett.* **111**, 226401 (2013).
 - [18] D.-T. Tran, A. Dauphin, N. Goldman, and P. Gaspard, *Phys. Rev. B* **91**, 085125 (2015).
 - [19] J.-N. Fuchs, R. Mosseri, and J. Vidal, *Phys. Rev. B* **98**, 165427 (2018).
 - [20] H. Huang and F. Liu, *Phys. Rev. Lett.* **121**, 126401 (2018).
 - [21] H. Huang and F. Liu, *Phys. Rev. B* **98**, 125130 (2018).
 - [22] R. Chen, C.-Z. Chen, J.-H. Gao, B. Zhou, and D.-H. Xu, *Phys. Rev. Lett.* **124**, 036803 (2020).
 - [23] D. Varjas, A. Lau, K. Pöyhönen, A. R. Akhmerov, D. I. Pikulin, and I. C. Fulga, *Phys. Rev. Lett.* **123**, 196401 (2019).
 - [24] I. C. Fulga, D. I. Pikulin, and T. A. Loring, *Phys. Rev. Lett.* **116**, 257002 (2016).
 - [25] S. Sakai, N. Takemori, A. Koga, and R. Arita, *Phys. Rev. B* **95**, 024509 (2017).
 - [26] K. Kamiya, T. Takeuchi, N. Kabeya, N. Wada, T. Ishimasa, A. Ochiai, K. Deguchi, K. Imura, and N. K. Sato, *Nat. Commun.* **9**, 154 (2018).
 - [27] S. Sakai and R. Arita, *Phys. Rev. Res.* **1**, 022002 (2019).
 - [28] R. N. Araújo and E. C. Andrade, *Phys. Rev. B* **100**, 014510 (2019).
 - [29] L. Guidoni, C. Triché, P. Verkerk, and G. Grynberg, *Phys. Rev. Lett.* **79**, 3363 (1997).
 - [30] M. A. Bandres, M. C. Rechtsman, and M. Segev, *Phys. Rev. X* **6**, 011016 (2016).
 - [31] J. Ledieu, J. T. Hoeft, D. E. Reid, J. A. Smerdon, R. D. Diehl, T. A. Lograsso, A. R. Ross, and R. McGrath, *Phys. Rev. Lett.* **92**, 135507 (2004).
 - [32] H. R. Sharma, M. Shimoda, A. R. Ross, T. A. Lograsso, and A. P. Tsai, *Phys. Rev. B* **72**, 045428 (2005).
 - [33] J. Ledieu, L. Leung, L. H. Wearing, R. McGrath, T. A. Lograsso, D. Wu, and V. Fournée, *Phys. Rev. B* **77**, 073409 (2008).
 - [34] J. A. Smerdon, J. K. Parle, L. H. Wearing, T. A. Lograsso, A. R. Ross, and R. McGrath, *Phys. Rev. B* **78**, 075407 (2008).
 - [35] S. Förster, K. Meinel, R. Hammer, M. Trautmann, and W. Widdra, *Nature (London)* **502**, 215 (2013).
 - [36] L. C. Collins, T. G. Witte, R. Silverman, D. B. Green, and K. K. Gomes, *Nat. Commun.* **8**, 15961 (2017).
 - [37] A. Y. Kitaev, *Phys.-Uspekhi* **44**, 131 (2001).
 - [38] V. Mourik, K. Zuo, S. M. Frolov, S. R. Plissard, E. P. A. M. Bakkers, and P. Kouwenhoven, *Science* **336**, 1003 (2012).
 - [39] S. Nadj-Perge, I. K. Drozdov, J. Li, H. Chen, S. Jeon, J. Seo, A. H. MacDonald, B. A. Bernevig, and A. Yazdani, *Science* **346**, 602 (2014).
 - [40] G. C. Ménard, S. Guissart, C. Brun, R. T. Leriche, M. Trif, F. Debontridder, D. Demaille, D. Roditchev, P. Simon, and T. Cren, *Nat. Commun.* **8**, 2040 (2017).
 - [41] H.-H. Sun, K.-W. Zhang, L.-H. Hu, C. Li, G.-Y. Wang, H.-Y. Ma, Z.-A. Xu, C.-L. Gao, D.-D. Guan, Y.-Y. Li, C. Liu, D. Qian, Y. Zhou, L. Fu, S.-C. Li, F.-C. Zhang, and J.-F. Jia, *Phys. Rev. Lett.* **116**, 257003 (2016).
 - [42] M. Sato, Y. Takahashi, and S. Fujimoto, *Phys. Rev. Lett.* **103**, 020401 (2009).
 - [43] M. Sato, Y. Takahashi, and S. Fujimoto, *Phys. Rev. B* **82**, 134521 (2010).
 - [44] J. D. Sau, R. M. Lutchyn, S. Tewari, and S. Das Sarma, *Phys. Rev. Lett.* **104**, 040502 (2010).
 - [45] J. Alicea, *Phys. Rev. B* **81**, 125318 (2010).
 - [46] S. N. Klimin, J. Tempere, J. T. Devreese, and D. van der Marel, *Phys. Rev. B* **89**, 184514 (2014).
 - [47] M. S. Scheurer and J. Schmalian, *Nat. Commun.* **6**, 6005 (2015).
 - [48] S. Gariglio, M. Gabay, J. Mannhart, and J.-M. Triscone, *Physica C* **514**, 189 (2015), superconducting Materials: Conventional, Unconventional and Undetermined.
 - [49] Y. Saito, T. Nojima, and Y. Iwasa, *Nat. Rev. Mater.* **2**, 16094 (2017).

- [50] E. I. Rashba, Sov. Phys. Solid State **2**, 1109 (1960).
- [51] E. I. Rashba and Y. A. Bychkov, JETP Lett. **39**, 78 (1984).
- [52] L. P. Gor'kov and E. I. Rashba, Phys. Rev. Lett. **87**, 037004 (2001).
- [53] A. V. Matetskiy, S. Ichinokura, L. V. Bondarenko, A. Y. Tupchaya, D. V. Gruznev, A. V. Zotov, A. A. Saranin, R. Hobara, A. Takayama, and S. Hasegawa, Phys. Rev. Lett. **115**, 147003 (2015).
- [54] L. J. Li, E. C. T. O'Farrell, K. P. Loh, G. Eda, B. Özyilmaz, and A. H. Castro Neto, Nature (London) **529**, 185 (2016).
- [55] S. L. Goertzen, K. Tanaka, and Y. Nagai, Phys. Rev. B **95**, 064509 (2017).
- [56] A. Soumyanarayanan, N. Reyren, A. Fert, and C. Panagopoulos, Nature (London) **539**, 509 (2016).
- [57] W. Han, Y. Otani, and S. Maekawa, npj Quant. Mater. **3**, 27 (2018).
- [58] R. Ghadimi, T. Sugimoto, and T. Tohyama, J. Phys. Soc. Jpn. **86**, 114707 (2017).
- [59] M. Arai, T. Tokihiro, T. Fujiwara, and M. Kohmoto, Phys. Rev. B **38**, 1621 (1988).
- [60] J. B. S. Mendes, O. Alves Santos, L. M. Meireles, R. G. Lacerda, L. H. Vilela-Leão, F. L. A. Machado, R. L. Rodríguez-Suárez, A. Azevedo, and S. M. Rezende, Phys. Rev. Lett. **115**, 226601 (2015).
- [61] Z. Wang, D.-K. Ki, H. Chen, H. Berger, A. H. MacDonald, and A. F. Morpurgo, Nat. Commun. **6**, 8339 (2015).
- [62] M. Gmitra and J. Fabian, Phys. Rev. B **92**, 155403 (2015).
- [63] P. G. de Gennes, *Superconductivity of Metals and Alloys* (Westview Press, Boulder, 1999).
- [64] D. J. Thouless, M. Kohmoto, M. P. Nightingale, and M. den Nijs, Phys. Rev. Lett. **49**, 405 (1982).
- [65] S. Fujimoto, Phys. Rev. B **77**, 220501(R) (2008).
- [66] E. D. B. Smith, K. Tanaka, and Y. Nagai, Phys. Rev. B **94**, 064515 (2016).
- [67] T. A. Loring, J. Math. Phys. **60**, 081903 (2019).
- [68] H. Huang and F. Liu, Phys. Rev. B **100**, 085119 (2019).
- [69] C.-K. Chiu, J. C. Y. Teo, A. P. Schnyder, and S. Ryu, Rev. Mod. Phys. **88**, 035005 (2016).
- [70] H. Tsunetsugu, T. Fujiwara, K. Ueda, and T. Tokihiro, Phys. Rev. B **43**, 8879 (1991).
- [71] A. Agarwala, S. Pai, and V. B. Shenoy, "Fractalized metals," (2018), arXiv:1803.01404 [cond-mat.dis-nn].
- [72] C. Caroli, P. D. Gennes, and J. Matricon, Phys. Lett. **9**, 307 (1964).
- [73] M. Chen, X. Chen, H. Yang, Z. Du, X. Zhu, E. Wang, and H.-H. Wen, Nat. Commun. **9**, 970 (2018).